Marjan Sedighi Gilani* and Francis W.M.R. Schwarze

Hygric properties of Norway spruce and sycamore after incubation with two white rot fungi

Abstract: In this study, changes in the hygroscopic properties of two main wood species for violin making, Norway spruce and sycamore, after treatment with *Physisporinus vitreus* and *Xylaria longipes* were investigated. Swelling and moisture sorption capacity of wood at the growth ring scale were visually and quantitatively assessed by thermal neutron radiography analysis. It was demonstrated that the fungal treatment improved the dimensional stability of both Norway spruce and sycamore, but also increased their moisture adsorption capacity. Dynamic vapor sorption tests and measurements of the changes in dimensions of the specimens in the laboratory were in good agreement with the results of neutron radiography analysis. The main difference between the moisture sorption of the untreated controls and treated wood was observed at high relative humidity, e.g., above 75%. The contradictory behavior of the increased hygroscopicity and reduced swelling was explained by selective degradation of the chemical components and condensation of the moisture content gained in the capillary voids that developed in the cell walls during fungal decay.

Keywords: dimensional stability, dynamic moisture sorption, neutron radiography, *Physisporinus vitreus*, resonance wood, violin making, wood decay fungi, *Xylaria longipes*

Introduction

Treatment with white rot fungus *Physisporinus vitreus* (Pers.) P. Karst. and *Xylaria longipes* Nitschke improved the acoustic properties of wood resonance via selective delignification of the cell walls, resulting in a reduction in density without significant alterations in the sound velocity and mechanical properties (Schwarze et al. 2008). *Physisporinus vitreus* also increases the liquid permeability of refractory wood species, mainly due to the preferential degradation of the pit membranes, a process known as bioincising (Schwarze 2007; Schwarze and Schubert 2011). Fungal treatment can lead to significant damage in the cell wall including the generation of small cavities (Lehringer et al. 2010). White rot fungi initially degraded lignin and hemicelluloses and later degraded cellulose (Martínez-Iñigo et al. 1999; Pandey and Pitman 2003; Ray et al. 2005; Schwarze 2007). Changes in the supramolecular architecture in the cell wall may entail a change of hygroscopicity and capacity of water adsorption (Kirk and Highley 1973).

The hygroscopicity in wood is studied by different techniques. Dynamic vapor sorption (DVS) is well suited for studying the sorption capacity and kinetics in native and modified wood (Hill et al. 2010, 2012; Xie et al. 2011). Optical and confocal laser scanning microscopy (CLSM) (Murata and Masuda 2001; Sakagami et al. 2007), environmental scanning electron microscopy (ESEM) (Gu et al. 2001; Ma and Rudolph 2006) and X-ray tomography (XRT) (Derome et al. 2010) are some characterization methods for *in-situ* studying of swelling or shrinkage in wood at the cellular level. Also, neutron radiography (NR) is better suited for quantitative moisture content (MC) estimation in wood than XRT (Zillig 2009) as it provides data with high resolution regarding water transport, even below the fiber saturation point (FSP) (Mannes et al. 2009; Sonderegger et al. 2010; Sedighi Gilani et al. 2012).

The main objective of the present study was to improve the understanding of the impact of controlled decay on the hygroscopicity of Norway spruce and sycamore wood (W_{spruce} and $W_{sycamore}$) as materials for violin construction. The hypothesis was that changes in the arrangement of the molecules of lignin, hemicelluloses and cellulose in the modified cell walls with fungi will alter the sorptivity and consequently the dimensional stability of wood. The modified material was characterized by NR, with a resolution that allows early wood (EW) and late wood (LW) layers to be distinguished. Traditional test methods were also applied for comparison. The goal was to elucidate, the equilibrium and also the time resolved distribution

*Corresponding author: Marjan Sedighi Gilani,** Applied Wood Laboratory, Swiss Federal Laboratories for Materials Science and Technology (Empa), Überlandstrasse 129, 8600 Dübendorf, Switzerland, e-mail: marjan.gilani@empa.ch
Francis W.M.R. Schwarze: Applied Wood Laboratory, Swiss Federal Laboratories for Materials Science and Technology (Empa), Lerchenfeldstrasse 5, CH-9014 St. Gallen, Switzerland

of adsorbed moisture and resulting swelling of untreated and modified wood with two species of wood decay fungi. The expectation was that the high resolution results concerning MC may contribute further improvement and standardization of the fungal modification processes for the treatment of wood resonance in musical instruments.

Materials and methods

Sample preparation and fungal incubation: 4 plates of $100 \times 2.5 \times 200$ mm³ (R×T×L) were planed from *Picea abies* L., W_{spruce} and 4 plates of the same dimensions from *Acer pseudoplatanus* L., $W_{sycamore}$ planks. Material was from a tree with narrow annualular rings, low LW fraction and low resin content, according to the criteria for quality resonance wood. Plates had no visible geometrical defects and were neighbors along the longitudinal direction. One plate from each species served as control and was climatized (20°C and 65% RH). The other three plates of W_{spruce} were incubated with *P. vitreus* and the 3 $W_{sycamore}$ with *X. longipes*, in different boxes, at 22°C and 70% RH according to the European Standard EN 113 (European Committee for Standardization 1997). The experiments were stopped after 8, 20 and 36 weeks by sterilizing the wood with ethylene oxide. Table 1 shows the density data of the woods before and after fungal treatment in equilibrium at 65% RH.

After treatment, specimens of $20 \times 2.5 \times 20$ mm³ (R×T×L) were quarter-sawn from each plate. They were examined by X-ray

Table 1 Duration of fungal treatment and changes in wood density.

Wood	Incubation time (week)	Initial density (kg m⁻³)	Density after processing (kg m⁻³)	Density loss (%)
Spruce	0 (contr.)	436	436	0
	8	440	430	2.3
	20	436	430	1.4
	36	438	431	1.6
Sycamore	0 (contr.)	582	582	0
	8	587	578	1.5
	20	585	565	3.4
	36	587	574	2.2

cone-beam computer tomography (3D-CT), to verify the absence of artifacts due to preparation. All specimens were oven dried for a week at 50°C, and at 80°C for the last 2 h, and then stored in a dry desiccator over silica gel.

Experimental procedure in neutron imaging setup: NR was performed at the NEUtron Transmission RAdiography (NEUTRA) beamline of the Paul Scherrer Institute (PSI), see Figure 1. The beamline was fed by the Swiss Neutron Spallation Source (SINQ) and provides neutrons with a thermal spectrum, at an energy level of 25 meV (Lehmann et al. 2001). The detector was of zinc sulfide containing 6 Li as neutron absorbing agent, with a thickness of 50 μm. The photons are led via a mirror onto a 16-bit CCD camera (2048×2048 pixels). The exposure time of NR was 34 s per image and the attained pixel size was in the magnitude of 44 μm/pixel.
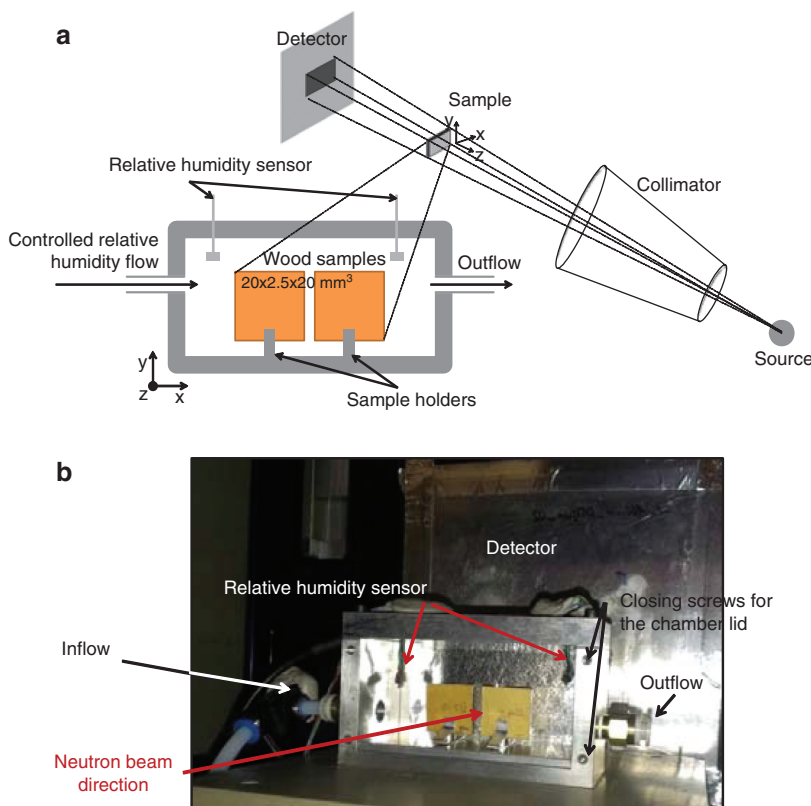

Figure 1 (a) Schematic overview of the neutron beamline and of the custom-made environmental chamber, (b) environmental chamber with open lid in the neutron imaging setup.

The custom-made environmental chamber was an aluminum enclosure, with two windows made of thin high-purity aluminum plates in the front and back. Due to the low attenuation coefficient of aluminum (0.1 cm^{-1} compared to 3.44 cm^{-1} for hydrogen), the interaction of the aluminum plate with neutrons and the induced error in quantitative image analysis was minimal. RH in the chamber was controlled by means of a humidity generator device. The RH (set at the lowest value 2%) was measured by sensors inside the chamber and recorded. Specimens were installed, side by side, on two aluminum grip holders, and the width (L direction) and height (R direction) were positioned on xy-plane of image acquisition. After acquiring few initial images of the dry specimens, RH was rapidly elevated to 80%, which was maintained over a period of 8 h. During this time, NR were recorded each 10 min. As reference for quantitative analysis, the mass of specimens was measured at the beginning and end of each experiment.

Analysis of neutron images: NR was based on intensity measurements of a neutron beam transmitted through an object. MC (kg m^{-3}) at the time t can be calculated from:

$$MC(t) = -\rho_L (z \cdot \Sigma_L) \ln(I(t)/I_{dry}) = \frac{\rho_L}{(z \cdot \Sigma_L)(\ln I_{dry} - \ln I(t))} \tag{1}$$

Where, ρ_L is the density of water, z is the specimen thickness, Σ is the attenuation coefficient of water, $I(t)$ is the intensity of the transmitted beam at time t and I_{dry} is the intensity at initial (dry) state (explained in detail in Sedighi Gilani et al. 2012). This means from 'subtraction' of current and initial images, the quantity of added moisture to the dry sample was calculated.

Swelling occurs in all three orthotropic directions of wood, stronger in the tangential than in the radial directions and weaker in the longitudinal direction (Skaar 1988). While the specimens expanded during moisture adsorption, the time resolved change in the geometry of specimen was documented with NR images. Swelling along the x-direction of the acquisition plane was determined as:

$$\varepsilon_x(y,t) = \frac{L_x(y,t) - L_x(y, t_0)}{L_x(y,t_0)} \tag{2}$$

where $\varepsilon_x(y, t)$ and $L_x(y, t)$ correspond with the time dependent swelling strain and the dimension of the specimen, both along x-axis at height position y and time t. As images were acquired in the 2D plane, only the swollen area (LR) of the specimens was available for evaluation. In each image this area was measured after segmentation from the background with Otsu's method (Otsu 1979).

Laboratory tests: To validate the reproducibility of the results from NR analysis in a larger group of specimens, different experiments were performed in the laboratory. Forty control and fungally incubated (8, 20 and 36 weeks) wood specimens with dimensions of 20×2.5×20 mm3 (R×T×L) were exposed to 80% RH in a climatic chamber at 20°C. Increase in mass and dimensions of the specimens were measured with a precision balance (Mettler Toledo, Switzerland, 0.0001 g) and caliper (PAV electronic, Switzerland, 0.01 mm) for 7 days, until they gained equilibrium MC (EMC). Also, sorption/desorption curves were measured in a DVS apparatus (TA instruments, Germany). It allows obtaining the precise isotherms over a stepwise variation of RH and a user set temperature range where isotherms were recorded. DVS tests were performed on 2 replicate specimens incubated for 36 weeks (W$_{36w, incub}$) and control (W$_c$) of Norway spruce and sycamore (total of eight tests). They were exposed to ten relative humidity steps in adsorption (5, 15, 25, 35, 45, 55, 65, 75, 85, 95%) and ten in desorption. RH was kept constant at each step, until moisture equilibrium was gained. For small tested wood specimens in DVS (<0.3 g dry mass), each step lasted between 2 h and 3 h, and for thin plates of wood tested in 80% RH climatic chamber, time of equilibrium lasted longer than 7 days. Contrary to the laboratory tests, the NR experiments represent the hygroscopic behavior of the material before gaining the equilibrium MC.

Results and discussions

Spatial distribution of moisture

In Figure 2 the orthogonal X-ray CT appearance of the W$_c$ and W$_{36w, incub}$ are shown in longitudinal-radial (LR), longitudinal-tangential (LT) and tangential-radial (TR) planes. LW layers can be distinguished from the EW by their lighter gray color. The very fine and parallel-aligned growth rings are typical for high quality resonance W$_{spruce}$. W$_{sycamore}$, however, the curly structure could have made the interpretation of the radiography (projection) images more difficult. Figures 3a and 4a show the NRs of the W$_c$ and W$_{36w, incub}$ in the dry state and after 1.5 h, 4 h and 8 h of moisture adsorption at 80% RH. The random intensity distribution pattern depends on the location of growth layers. Warm colors correspond to low neutron attenuation (low
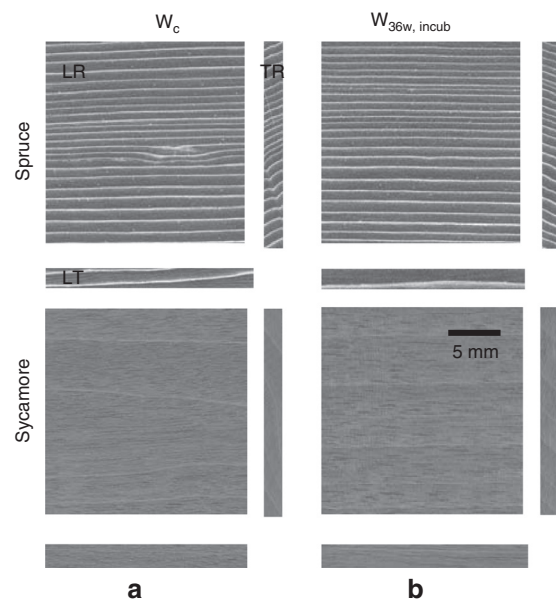

Figure 2 X-ray computer tomography (3D-CT) showing the orthogonal appearance of untreated and treated wood in the LR, LT and RT planes. N.B., slices were from the center of test specimens. Top: (a) untreated control and (b) Norway spruce specimen after 36 weeks' incubation with *Physisporinus vitreus*. Bottom: (a) untreated control and (b) sycamore specimen after 36 weeks' incubation with *Xylaria longipes*.
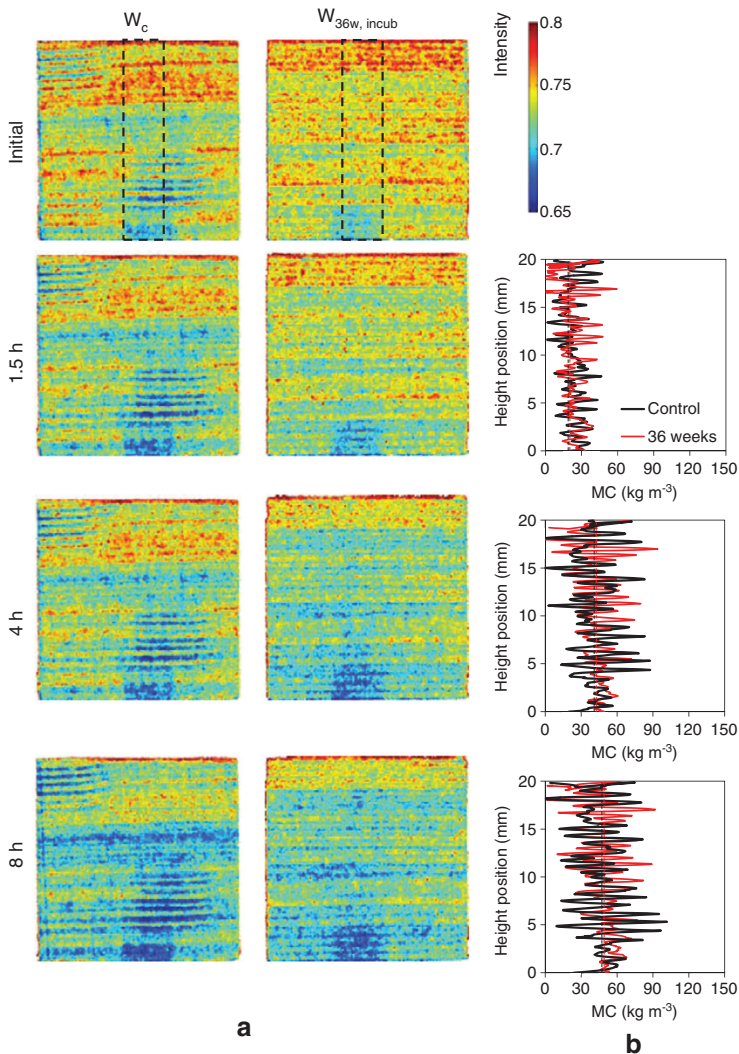
Figure 3 (a) Neutron transmission images showing the change of the intensity in control specimen of Norway spruce and specimen after 36 weeks' incubation with *Physisporinus vitreus,* (b) profiles of the MC in ROI, (2 mm width in the center).

MC), which changed to cold colors with moisture sorption. More bluish colors in the location of sample holders are artifacts, due to the increased attenuation of neutron beam by aluminum.

For interpretation of the gray value intensity pattern and its spatial changes in time of exposure to the humid air, differences in density, porosity and moisture capacity of EW and LW layers must be taken into account. More extended distribution of cold colors in $W_{spruce,}$ EW layers was due to thin tracheids walls, larger lumina, and a larger number of pits than in LW. It makes the EW layers more permeable to the vapor and the preferential paths for vapor transport (Zillig 2009). Changes in the intensity of the neutron beam was due to the 'change' of the water mass in the specimens. In Spruce, the extent of cold colors variation within the EW and LW layers in the W_c was more

pronounced, compared with the $W_{36w, incub}$, which indicated a more significant difference between the hygroscopic properties of growth layers in W_c. This trend was not clearly observed in curly $W_{sycamore}$, as the growth layers were not perpendicular to the plane of image acquisition (LR plane), as apparent in X-ray orthogonal slices in Figure 2.

From Equation 1, the 'absolute' quantity of the MC can be determined by comparing the image of time t and the initial state. For this comparison, change in the dimensions of the specimens (swelling) should be registered. However, a faultless registering of the whole surface of the specimen in fine-grain resonance wood was challenging. Thus in Figures 3b and 4b, the profiles of the MC, only the illustrated region of interest (ROI) were compared. The vertical axis corresponds to the specimen height and the horizontal axis showed the MC, obtained by averaging the
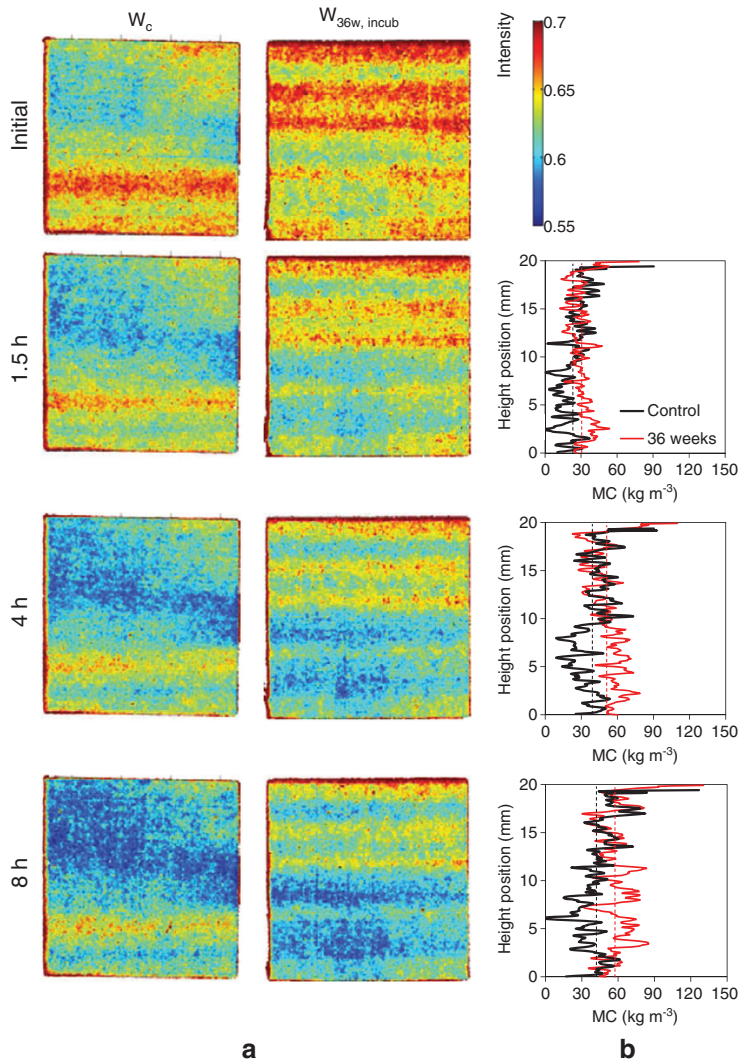
Figure 4 (a) Neutron transmission images for control specimen of sycamore and specimen after 36 weeks' incubation with *Xylaria longipes*, (b) profiles of the MC in ROI, (2 mm width in the center).

quantified moisture in ROIs at different sorption states. The moisture profiles are illustrated by black solid lines for W_c and red solid lines for $W_{36w, incub}$. Vertical dashed lines indicate the average of the altered MCs across the growth layers (black for W_c and red for W_{incub}).

In spruce, MC profiles of W_c and $W_{36w, incub}$ were not significantly different. In contrast, the MC profile of $W_{36w, incub}$ showed a higher moisture capacity than W_c in sycamore, even after a few hours. The MC profile altered across the grain depends on the location of EW and LW layers. Figure 5 shows the average grain MC alteration, in columns of horizontal strip fillers for the W_c and diagonal patterns for $W_{36w, incub}$. Also, variance of the grain MC alteration in the ROI is indicated by black solid lines for the W_c and red solid lines for $W_{36w, incub}$. Moisture capacity of both wood species increased after fungal treatment. One main observation

was the lower variance of the grain MC in $W_{36w, incub}$. This was interpreted as a less different moisture capacity of the EW and LW layers in $W_{36w, incub}$, indicating a more homogeneous sorption behavior at growth ring scale. The variance of the grain MC alteration in W_{spruce} was higher than in $W_{sycamore}$. Less variable profiles of MC in $W_{sycamore}$ may have been related to its diffuse-porous microstructure when compared with W_{spruce}, as indicated in Figure 6. This figure, acquired at synchrotron XRT microscopy with TOMCAT beamline of PSI, compared the 3D structures and the anatomical features such as EW and LW cells, xylem rays, vessels and hyphae inside the cell lumina in W_{spruce} and $W_{sycamore}$, after 36 weeks' incubation. However, the less variable profiles of MC may have been related to the morphology of the grains in the TR plane. As explained above, the orientation of 'curly' growth rings was not exactly
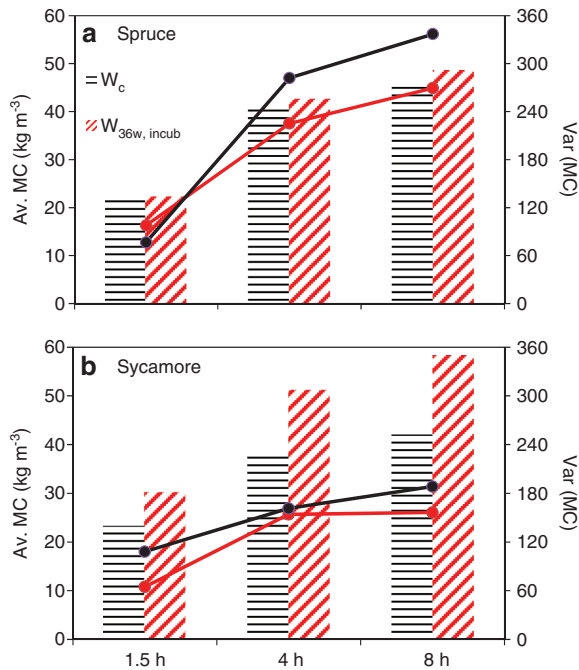
Figure 5 Average and variance of alternation in the grain MC in the ROI, in control and 36 weeks' fungally incubated (a) spruce and (b) sycamore.

perpendicular to the neutron beam, thus the radiography images projected a combination of EW and LW layers.

Temporal change of MC and swelling

From each NR, the total MC of the specimens was calculated by adding the obtained MC from NR for each pixel, over the total area of each specimen. Figure 7a,b show the temporal increase of the mass MC (%) at 80% RH, after

dividing the calculated quantity of the moisture from Equation 1 by the specific density of each specimen. Also, in Figure 7c and d, the swelling strains in the RL plane are compared. Both wood specimens were incubated for 8, 20 and 36 weeks with *P. vitreus* and *X. longipes*. The average difference of the MC was measured with the precision balance at the end of experiments. The calculated data from NR was <7.1%. This error was in an acceptable range (Hassanein 2006) and confirmed the applicability of the explained procedure above for quantitative NR analysis.

The coinciding variation of the slope of MC and swelling curves confirms their relationship. After 4 h, this slope significantly decreased, indicating the higher capacity of both W_c and W_{incub} for moisture adsorption at the start of the experiment. Even though, none of the test specimens gained the equilibrium MC after 8 h. Spruce and sycamore showed different sorption capacities. After 8 h sorption, the MC in the control W_{spruce} reached 10.3% whereas in $W_{sycamore}$, the MC was 8.2% (20% lower). Likewise, swelling of the control W_{spruce} at the end of the experiment was 2.2%, whereas $W_{sycamore}$ swelled 2.0%. After fungal incubation, moisture adsorption in both wood species increased, however, unexpectedly, swelling occurred with a lower rate in the $W_{36w, incub}$. In Figure 8, MCs after an 8 h sorption test are presented as black columns and the corresponding swelling strains are shown as red lines. The increasing trend of the moisture capacity and dimensional stability (i.e., reduced swelling) of $W_{36w, incub}$ is clearly visible as a function of incubation time.

Equilibrium MC in the laboratory

Figure 9 shows the averaged EMCs of the samples as black columns and corresponding swelling by red lines. The
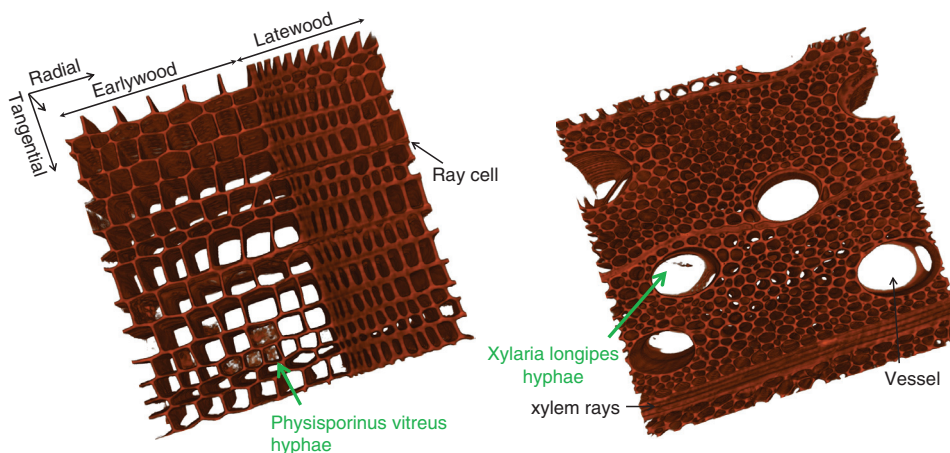

Figure 6 Full micro-tomography image of Norway spruce (left) and sycamore wood (right), after 36 weeks' incubation with *Physisporinus vitreus* and *Xylaria longipes*.
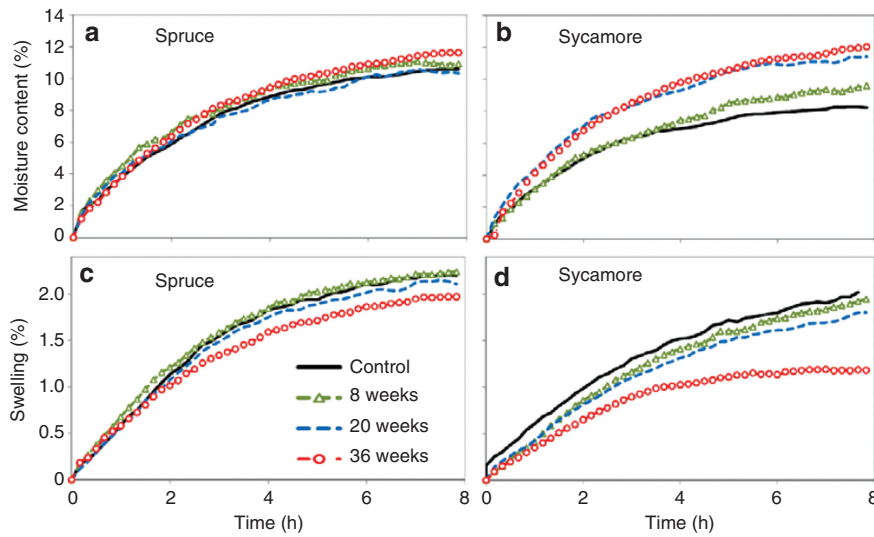
Figure 7 Time resolved moisture adsorption (a-b) and corresponding swelling in the plane of image acquisition (c-d) for controls and specimens incubated for 8, 20 and 36 weeks with fungus.

positive slope of the EMCs trend line indicates the increase of the sorption capacity as a function of incubation time. Also, swelling of the W_{incub} was less than the controls and decreased with incubation time, which confirms the results from NR analysis.

Figure 10a and b show the results from DVS tests of the W_c and $W_{36w, incub}$ exposed to 10 RH steps in adsorption and 10 steps in desorption. The isotherms exhibited typical hysteresis (MC is higher in desorption than in sorption). Thick lines correspond to the hysteresis behavior of W_c,
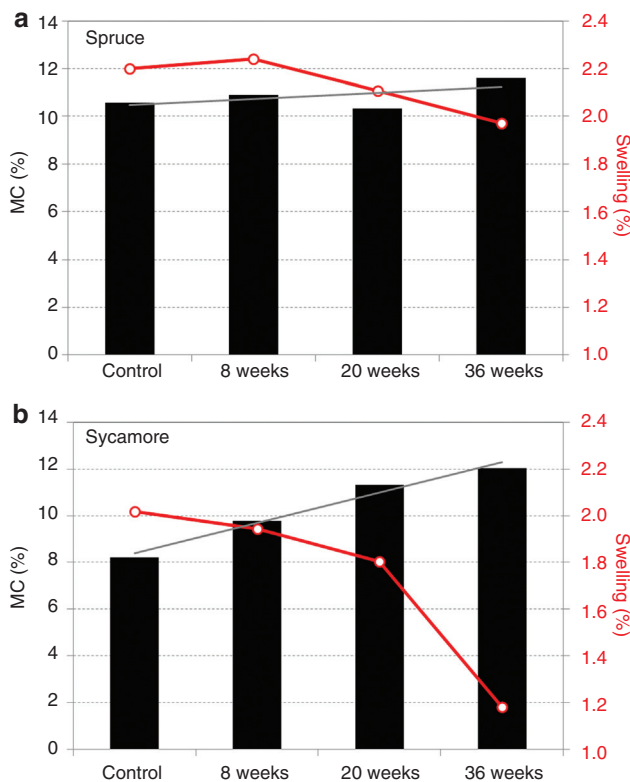

Figure 8 MC of controls and fungally (8, 20 and 36 weeks) incubated Norway spruce (a) and sycamore wood (b) in black columns and corresponding swelling in red lines after 8 h exposure to 80% RH.
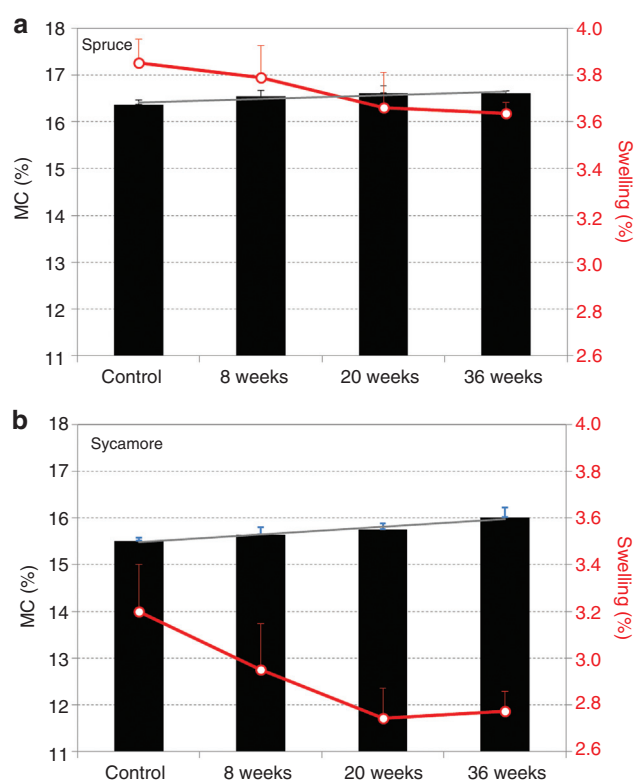
Figure 9 EMC and swelling (red lines in secondary vertical axes) of controls and fungally treated Norway spruce (a) and sycamore wood (b).
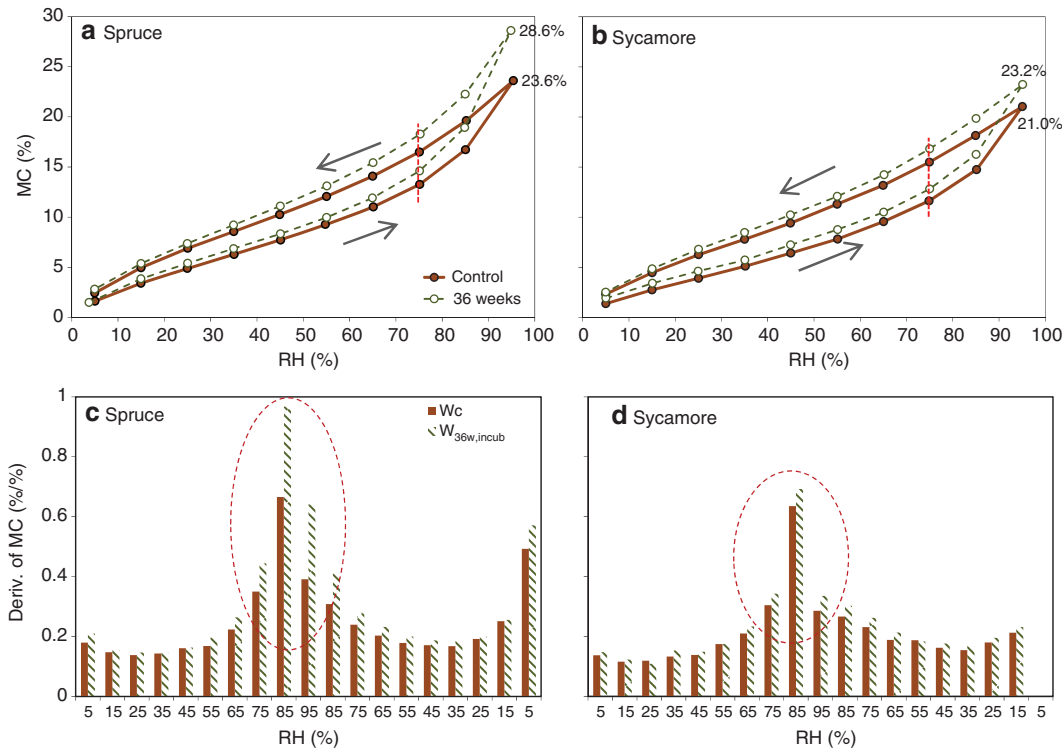
Figure 10 Measured isotherm in dynamic vapor sorption apparatus for control and 36 weeks' fungally incubated Norway spruce (left, a) and sycamore wood (right, b) and their first derivatives (bottom, c and d).

and dashed lines indicate the behavior of $W_{36w, incub}$. The slope of the isotherms for $W_{36w, incub}$ increased at RHs above 75%, whereas below that value, the hygroscopicity of both materials was comparable. For example in spruce, EMC of W_c at 65% RH was 11% that was 8% lower than in $W_{36w, incub}$. EMC of W_c at 95% RH was 23.6%, while it was increased to 28.6% in $W_{36w, incub}$. In Figure 10c and d, the first derivatives of EMCs, with respect to the change of RH are presented. It highlights the higher moisture capacity of both fungally treated woods compared with W_c at RHs above 75%.

These observations attribute to the degradation and change in the wood cell wall constituents after modification with white rot fungi. More specifically, spruce incubated with *P. vitreus* resulted in a preferential degradation of the pit membranes and delignifcation of the secondary walls (Schwarze 2007; Lehringer et al. 2011a,b). In sycamore, *X. longipes* causes cell wall erosion that starts commonly in the secondary walls of libriform wood fibers (Schwarze et al. 2008). Partial degradation of the cell wall substances may increase the sorption capacity of wood by increasing the accessibility of cellulose fibrils to the water molecules. The contradictory behavior of the fungally treated wood, i.e., increase in the moisture capacity and dimensional stability can be explained by the hypothesis that the gained moisture is not totally bound to the cell

walls. Probably, a fraction of water molecules condensate in the developed voids induced during fungal decay. These voids are within the range of 2–5 nm (Flournoy et al. 1993), and their volume fraction must be correlated with the mass loss in the material after fungal treatment. Nevertheless, the differences in moisture capacity of the W_c and W_{incub} were more significant in spruce than in sycamore with a higher mass loss. Condensation in such capillaries, based on Kelvin equation may take place even if the ambient atmosphere is not fully saturated with water vapor (Skaar 1988). Thus the voids will act as micro-sinks for vapor condensation, which increase the equilibrium MC of the incubated woods at RHs above certain limits. This is confirmed by DVS test results, i.e., the higher sorption capacity of the fungal treated wood after RH exceeded, e.g., 75%. Degradation of cellulose fibrils in the cell walls of fungal treated wood for periods longer than 8 weeks (Lehringer et al. 2011b) can be another explanation for the improved dimensional stability of the modified wood.

NR analysis showed that the alteration of MC across the grain was less significant in the W_{incub} (Figure 5). More abundant development of voids in the thick walls of LW after fungal treatment (Lehringer et al. 2010) may lead to a similar hygroscopic behavior as observed in EW, by increasing their porosity. It may also result in improved

dimensional stability of W_{incub}, as LW generally showed higher swelling strains in sorption. This minimized the generation of internal stresses in the material that corresponded with different swelling/shrinkage of EW and LW (Jakiela et al. 2008; Neimsuwan et al. 2008).

Conclusions

Processing Norway spruce and sycamore wood with *P. vitreus* and *X. longipes* reduces the density, improves the dimensional stability and elevates the moisture sorption capacity. Moreover, the variance in sorption behavior of the EW and LW regions are reduced, thus the mesoscopic hygroscopic behavior of wood became more homogeneous. The hygroscopicity changes after fungal incubation was successfully studies by thermal NR analysis. DVS tests and the mass gain of dry samples exposed to 80% RH confirm the NR results. It is possible that water molecules condensate in fungally induced nano-voids in the cell walls of incubated wood. Probably, the condensed water in the voids does not essentially affect the dimensional stability of wood. As a result, the new properties of the fungally treated spruce and sycamore wood make them more suitable for application as top and bottom-plates of violins.

References

Derome, D., Griffa, M., Koebel, M., Carmeliet, J. (2010) Hysteretic swelling of wood at cellular scale probed by phase-contrast X-ray tomography. J. Struct. Biol. 173:180–190.

European Committee for Standardization. European Standard EN 113. Wood preservatives: test method for determining the protective effectiveness against wood destroying basidiomycetes. Determination of toxic values. Brussels, Belgium: European Committee for Standardization 1997.

Flournoy, D.S., Paul, J.A., Kirk, T.K., Highley, T.L. (1993) Changes in the size and volume of pores in sweetgum wood during simultaneous rot by *Phanerochaete chrysosporium* burds. Holzforschung 47:297–301.

Gu, H., Zink-Sharp, A., Sell, J. (2001) Hypothesis on the role of cell wall structure in differential transverse shrinkage of wood. Holz Roh- Werks. 59:436–442.

Hassanein, R. (2006) Correction methods for the quantitative evaluation of thermal neutron tomography. Dissertation, ETH Zurich.

Hill, C.A.S., Norton, A.J., Newman, G. (2010) The water vapour sorption properties of Sitka spruce determined using a dynamic vapour sorption apparatus. Wood Sci. Technol. 44:497–514.

Hill, C.A.S., Ramsay, J., Keating, B., Laine, K., Rautkari, L., Hughes, M., Constant, B. (2012) The water vapour sorption properties of thermally modified and densified wood. J. Mater. Sci. 47:3191–3197.

Jakiela, S., Bratasz, L., Kozlowski, R. (2008) Numerical modeling of moisture movement and related stress field in lime wood subjected to changing climate conditions. Wood Sci. Technol. 42:21–37.

Kirk, T.K., Highley, T.L. (1973) Quatitative Changes in structural components of conifer woods during decay by white- and brown-rot fungi. Phytophatology 63:1338–1342.

Lehmann, E., Vontobel, P., Wiezel P.L. (2001) Properties of the radiography facility NEUTRA at SINQ and its potential for use as European reference facility, Nondestr. Testing Eval. 16:191–202.

Lehringer, C., Hillebrand, K., Richter, K., Arnold, M., Schwarze, F., Militz, H. (2010) Anatomy of bioincised Norway spruce wood. Int. Biodet. Biodegrad. 64:346–355.

Lehringer, C., Koch, G., Adusumalli, R.B., Mook, W.M., Richter, K., Militz, H. (2011a) Effect of Physisporinus vitreus on wood properties of Norway spruce. Part 1: aspects of delignification and surface hardness. Holzforschung 65:711–719.

Lehringer, C., Saake, B., Zivkovic, V., Richter, K., Militz, H. (2011b) Effect of physisporinus vitreus on wood properties of Norway spruce. Part 2: aspects of microtensile strength and chemical changes. Holzforschung 65:721–727.

Ma, Q., Rudolph, V. (2006) Dimensional change behavior of Caribbean pine using an environmental scanning electron microscope. Drying Technol. 24:1397–1403.

Mannes, D., Sonderegger, W., Hering, S., Lehmann, E., Niemz, P. (2009) Non-destructive determination and quantification of diffusion processes in wood by means of neutron imaging. Holzforschung 63:589–596.

Martínez-Iñigo, M., Immerzeel, P., Gutierrez, A., Carlos del Río, J., Sierra-Alvarez, R. (1999) Biodegradability of extractives in sapwood and heartwood from scots pine by sapstain and white rot fungi. Holzforschung 53:247–252.

Murata, K., Masuda, M., (2001) Observation of microscopic swelling behaviour of the cell wall. J. Wood Sci. 47:507–509.

Neimsuwan. T., Wang, S., Taylor, A.M., Rials, T.G. (2008) Statics and kinetics of water vapor sorption of small loblolly pine samples. Wood Sci. Technol. 42:493–506.

Otsu, N.A. (1979) A threshold selection method from grey-level histograms. IEEE T Syst. Man Cyb. 9:62–66.

Pandey, K.K., Pitman, A.J. (2003) FTIR studies of the changes in wood chemistry following decay by brown-rot and white-rot fungi. Int. Biodet. Biodegrad. 52:151–160.

Ray, M., Kleist, G., Murphy, R. (2005) Decay assessment in a hardwood handrail at the South Bank, London. J. Int. Wood Sci. 17:51–58.

Sakagami, H., Matsumura, J., Kazuyuki, O. (2007) Shrinkage of tracheid cells with desorption visualized by confocal laser scanning microscopy. IAWA J. 28:29–37.

Schwarze, F.W.M.R. (2007) Wood decay under the microscope. Fungal Biol. Rev. 1:133–170.

Schwarze, F.W.M.R., Schubert M. (2011) Physisporinus vitreus: a versatile white-rot fungus for engineering value added wood products. Appl. Microbiol. Biotechnol. 92:431–440.

Schwarze, F.W.M.R., Spycher, M., Fink, S. (2008) Superior wood for violins – wood decay fungi as a substitute for cold climate. New Phytol. 179:1095–1104.

Sedighi Gilani, M., Griffa, M., Mannes, D., Lehmann, E., Carmeliet, J., Derome, D. (2012)Visualization and quantification of liquid water transport in softwood by means of neutron radiography. Int. J. Heat Mass Transfer. 55:6211–6221.

Skaar, C. (1988) Wood-water relations. Springer-Verlag Berlin, Germany.

Sonderegger, W., Hering, S., Mannes, D., Vontobel, P., Lehmann, E., Niemz, P. (2010) Quantitative determination of bound water diffusion in multilayer boards by means of neutron imaging. Eur. J. Wood Prod. 68:341–350.

Xie, Y., Hill, C.A.S., Hill, Xiao, Z., Mai, C., Militz, H. (2011) Dynamic water vapour sorption properties of wood treated with glutaraldehyde. Wood Sci. Technol. 45:49–61.

Zillig, W. (2009) Moisture transport in wood using a multi-scale approach, PhD Thesis, Catholic University of Leuven, Belgium.